Characterization of Turbulent Flow in a Breakup Cell.

Vejražka, Jiří
2016

EFM16 Experimental Fluid Mechanics 2016
Mariánské Lázně 15th - 18th November 2016

Characterization of turbulent flow in a breakup cell

Jiří Vejražka[1,a], *Mária* Zedníková[1], and *Petr* Stanovský[1]

[1]Institute of Chemical Process Fundamentals, Department of Multiphase Reactors, 16502 Praha, Czech Republic

Abstract. Our research focuses on breakup of bubbles and drops induced by a flow turbulence. In this contribution, we describe the experimental setup used for studying the breakup, and we characterize flow within it. The setup is a rectangular glass cell, in which a turbulent flow is generated by a set of coaxial nozzles. The flow within it is characterized by means of particle image velocimetry. From the velocity data, i) local dissipation rate (ε) is estimated using Large-Eddy PIV method, and ii) statistics of velocity difference in two points is evaluated. Estimation of ε is validated by integrating the total dissipation in the setup, which reasonably agrees with the injected kinetic energy. The probability density function of velocity difference is non-Gaussian and when properly normalized, it is universal within the setup.

1 Introduction

Bubbly flows or a flows of two immiscible liquids are types of flow, which are encountered in industrial applications (e.g. boilers, water treatment plants, crude-oil processing etc.), but which are quite difficult to be modelled numerically. Usually, the detailed motion of individual bubbles or drops (thereinafter *particles*) cannot be solved due to limited computational resources. Most of simulations therefore computes an average velocity and number density of particles in a given computational cell. For computing interactions with the continuous fluid, various forces acting between them (drag, added-mass force, history force) has to be evaluated. This requires knowledge of particle sizes. In most simulations, single (and fixed) particle size, estimated somehow, is assumed. In this aspect, the simulations considerably differ from reality, where the size distribution of particles is quite broad and is evolving along the flow due to breakup of particles and their coalescence.

To reflect better the reality of size distribution of particles in flow, approaches incorporating *population-balance modelling* are being developed [1], [2]. This development is hindered, however, by the required knowledge about the breakup and coalescence of particles.

Concerning the breakup, numerous models for breakup frequency and size distribution of daughter particles have been proposed and they are reviewed e.g. in [2] or [3]. A difficulty in development of these models consists in the fact that there is a largely insufficient amount of experimental data suitable for their validation. Though experimental investigations of the breakup are relatively numerous, most of them focuses on the breakup in agitated vessel, either real ones (e.g. [4]), or approximated by a channel flow obstructed by a single-blade (e.g. [5], [6]). While such data are suitable for modelling of agitated vessels, they can hardly be used for validation of breakup models themselves owing to complicated and inhomogeneous flow. Experiments with better defined flows (e.g. [7-11]) are much less numerous, and they generally provides a relatively limited set of data.

In our work, we carried out experiments, which should provide additional experimental data on bubble breakup. The experiments were designed in the way that we can characterize the flow. Other objective is the ability to acquire large amount of breakups to allow its statistical treatment.

In this contribution, we describe the experimental setup and we characterize the turbulent flow within it. In the companion paper [12], we discuss methods used for bubble tracking and breakup detection, and we report on experimental observation of breakups themselves.

2 Experimental setup and methods

2.1 Experimental channel

The experiments are carried out in a rectangular glass cell with the downward water flow (Figure 1); the channel has cross-section 44x88 mm^2 and height 250 mm. The turbulent flow is generated by an array of injectors, arranged in a 3x6 rectangular grid with spacing 14.6 mm. Each injector is composed of two coaxial nozzles. The diameter of inner nozzle is 4.2 mm. The outer nozzle has a cross-section in shape of an annulus with inner and outer diameters 6.5 and 9.2 mm, respectively. In bottom, liquid leaves the cell through a plate with 18 holes (diameter 9.2 mm, arranged in 6x3 grid with 14.6 mm spacing). In the bottom part of the cell, there is a tube for injecting either air bubbles or drops of an immiscible liquid.

[a] Corresponding author: vejrazka@icpf.cas.cz

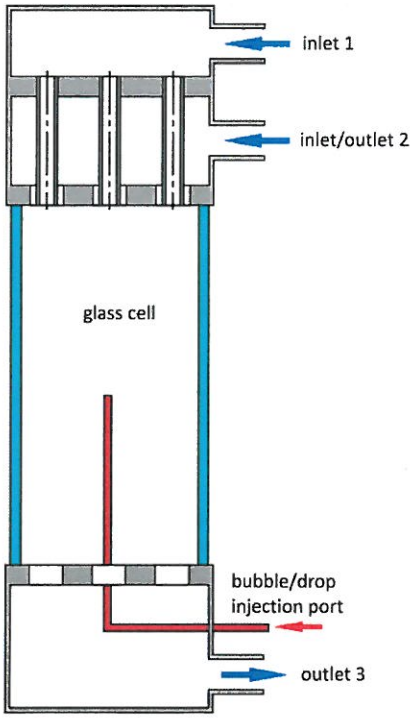

Fig. 1. Scheme of the experimental cell

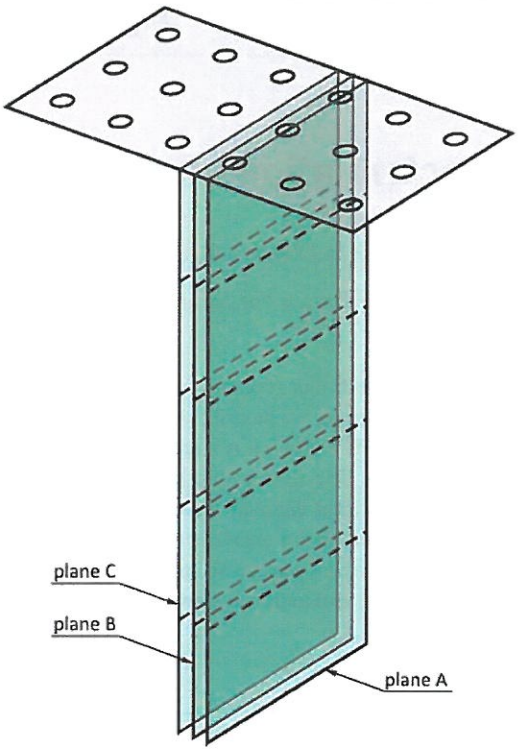

Fig. 2. Scheme of measurement planes

2.2 Experimental conditions

The mean liquid velocity in the cell is controlled by adjusting appropriately the flow rate through outlet 3 (Fig. 1). In most experiments reported here and in the companion paper, the outlet flow rate is $Q_3 = 48$ L/min, and the mean velocity in the cell is then 20 cm/s (which is close to the rise velocity of a bubble in water). The turbulence level can be adjusted by setting the ratio of flow rates in the inlet 1 (Q_1) and inlet/outlet 2 ($Q_3 - Q_1$). Measurements were done for inlet flow rate Q_1 of 20, 48, 68 and 88 L/min; in the latter two cases, the second port is effectively an outlet.

The used liquid is distilled water, whose temperature is maintained at 23°C. If not stated otherwise, results reported here are for $Q_1 = 68$ L/min. Results for this flow rate are taken as an illustrative example. The character of results for other flow rates is quite similar.

2.2 Measurements of the velocity field

The instantaneous velocity field is characterized by means of particle image velocimetry (PIV). The PIV measurements were carried out in three different planes, as schematized in Fig. 2. Plane A was placed below centers of third row of nozzles; plane C was placed between two rows of nozzles, and the last plane (B) was just in between of the other two planes. For measurement in each plane, the camera and laser were moved downward to five different vertical positions in order to cover sufficiently large part of the experimental cell.

PIV images are treated using in-house software PIVsuite [13], which has been previously validated using PIVchallange [14] data sets. Additional details about velocity field measurements are provided in Tab. 1.

2.3 Estimation of turbulent dissipation rate

Most of models for particle breakup use the local dissipation rate of turbulent energy ε as a parameter, by which the flow turbulence is characterized [4]. The local dissipation rate cannot be deduced directly from the measurements, because the spatial resolution of PIV (between 0.5 and 1.4 mm) is insufficient to resolve dissipating eddies (Kolmogorov scale is estimated to be in range 10 to 50 μm). Therefore, Large-Eddy PIV method [15], which is an equivalent of LES method [16] used for numerical simulations, has been used.

The method is adopted in the way detailed by de Jong et al. [17]. The dissipation rate is estimated as

$$\varepsilon = 2C_S^2 \Delta^2 \left\langle \left\| \hat{s}_{ij} \right\| \hat{s}_{ij} \hat{s}_{ij} \right\rangle, \qquad (1)$$

where C_S is the Smagorinsky constant (standard value 0.17 is used). Δ is the size of filter, which converts the real-world values to those experimentally observed by PIV method (denoted by the cap). A series of tests suggest that the vector spacing (0.52 mm) is the appropriate filter size for present experiments. The stress tensor $\hat{s}_{ij}$ cannot be evaluated completely because of unknown velocity components and unknown derivatives in 2D-2C measurements. The tensor dot product is therefore estimated as

Table 1. Parameters of PIV measurements.

Type	2D-2C (two-dimmensional, two velocity components)
Laser	Quantronix Darwin Duo (Nd-YLF laser, 527 nm, up to 25 mJ)
Laser Sheet optics	Dantec Dynamics, sheet thickness approx. 0.8 mm
Camera	Photron FastCam SA1.1 (1 MPx at 5 400 frames per second)
Lens	Nikon AF Micro-Nikkor 60mm f/2.8D, protected by low-pass filter (> 532 nm)
Seeding	Microparticles GmbH, PMMA-Rhodamine B fluorescent particles, size range 1-20 μm and 20-50 μm, about 0.1 mL of suspension per 1 L of liquid
number of image pairs	1000 (decorrelated) for each measurement position
Software	PIVsuite
PIV processing parameters	number of passes: 4 final interrogation area size: 32x32 px vector spacing: 12x12 px image deformation: bi-cubic spline image interpolation: logarithmic validation: floating median test peak interp.: 2x3 points, logarithmic
Spatial resolution	43.2 μm/px vector spacing: 0.52 mm interrogation area size: 1.38 mm
Temporal resolution	Δt between images in pair: $\Delta t = 200\mu s$ Δt between image pairs: $\Delta t > 10$ ms

$$\hat{s}_{ij}\hat{s}_{ij} \approx 2\left(\frac{\partial \hat{u}}{\partial x}\right)^2 + 2\left(\frac{\partial \hat{w}}{\partial z}\right)^2 + 2\left(\frac{\partial \hat{u}}{\partial x}\frac{\partial \hat{w}}{\partial z}\right) + \frac{3}{2}\left(\frac{\partial \hat{w}}{\partial z} + \frac{\partial \hat{u}}{\partial x}\right)^2, \quad (2)$$

where indices u and w are the horizontal and vertical velocity components, respectively, seen in the xz plane illuminated by the laser. The norm in (1) is defined

$$\left\|\hat{s}_{ij}\right\| = \sqrt{\hat{s}_{ij}\hat{s}_{ij}} \quad (3)$$

and broken brackets in (1) is time-averaging. The dissipation rate is computed for each image pair.

2.4 Statistics on velocity difference

The breakup of fluid particle is supposed to depend on the difference of velocity, which the bubble feels across its diameter [7]. We evaluate the longitudinal and transversal velocity differences δu and δw, respectively, as

$$\delta u = u(x, z+\frac{d}{2}) - u(x, z-\frac{d}{2}),$$
$$\delta w = w(x, z+\frac{d}{2}) - w(x, z-\frac{d}{2}), \quad (4)$$

where $u(x,z)$ and $w(x,z)$ are the horizontal and vertical velocity components in position (x,z), respectively, and d is the distance, for which the velocity difference is evaluated.

In practice, samples of δu and δw (taken in different times and positions) are regarded as a random variable and we are interested in their probability density functions (p.d.f.). To improve the statistical convergence, we assume that these densities depend only on vertical position z. The set of δu and δw data is hence taken over all times, all horizontal positions, and moreover for all points laying in the layer, which was 2.6 mm thick (i.e. 5 velocity vectors).

3 Results and discussion

3.1. General character of the velocity field

General character of the velocity field is demonstrated in Fig. 3, which shows the mean vertical velocity, fluctuating vertical velocity and local dissipation rate. These measurements are from the plane A and for conditions, when the inflow 1 and outflow 3 were 68 L/min and 48 L/min, respectively. Figure 4 then show corresponding profiles in a standard form of plot. Apparently, the character of jet flow is pertained till about z = 60 mm. For different flow velocities, character of the velocity field is quite similar.

3.2. Rate of dissipation of turbulent energy

The dissipation rate ε of turbulent energy, estimated from measured velocity fields, is also shown in Figs. 2 and 3. For evaluation of breakup experiments, the dissipation rate is averaged over same vertical positions. Such an average value is shown in Fig. 5 by the red line.

These measurements of ε are carried out also in the other two measurement planes, for which ε is also averaged. These resulting downstream decays of ε are shown in Figure 5 by green and blue lines. Finally, the profiles of the dissipation rate from the three measurement planes are again averaged, leading to a mean dissipation rate as a function of vertical position $\varepsilon_{avg}(z)$, which is shown by the black line.

These estimations of ε are repeated for four different flow rates Q_1 of the inlet 1 (whereas the flow rate in outlet 3 was kept constant at Q_3 = 48 L/min). The resulting vertical profiles of $\varepsilon_{avg}(z)$ are shown in Fig. 6. Apparently, the dissipation rate is affected by the ratio of flow rates Q_1/Q_3. The results shown in this figure are the final results, which are then used for interpretation of the bubble breakup experiments in the breakup cell. These averaged values are useful only for $z > 60$ mm, because closer to nozzles, the dissipation rate ε across the cross-section of the experimental cell is not uniform and hence is not represented correctly by its averaged value.

It is difficult to validate the estimation of the local dissipation rate using the LEPIV method, because there are no suitable independent techniques for its estimation. Integral energy balance can be tested by comparing the total dissipation rate ($\rho\varepsilon$ integrated over volume of the cell) to the influx of the kinetic energy through inlets. Such a comparison is justified by dimensional arguments

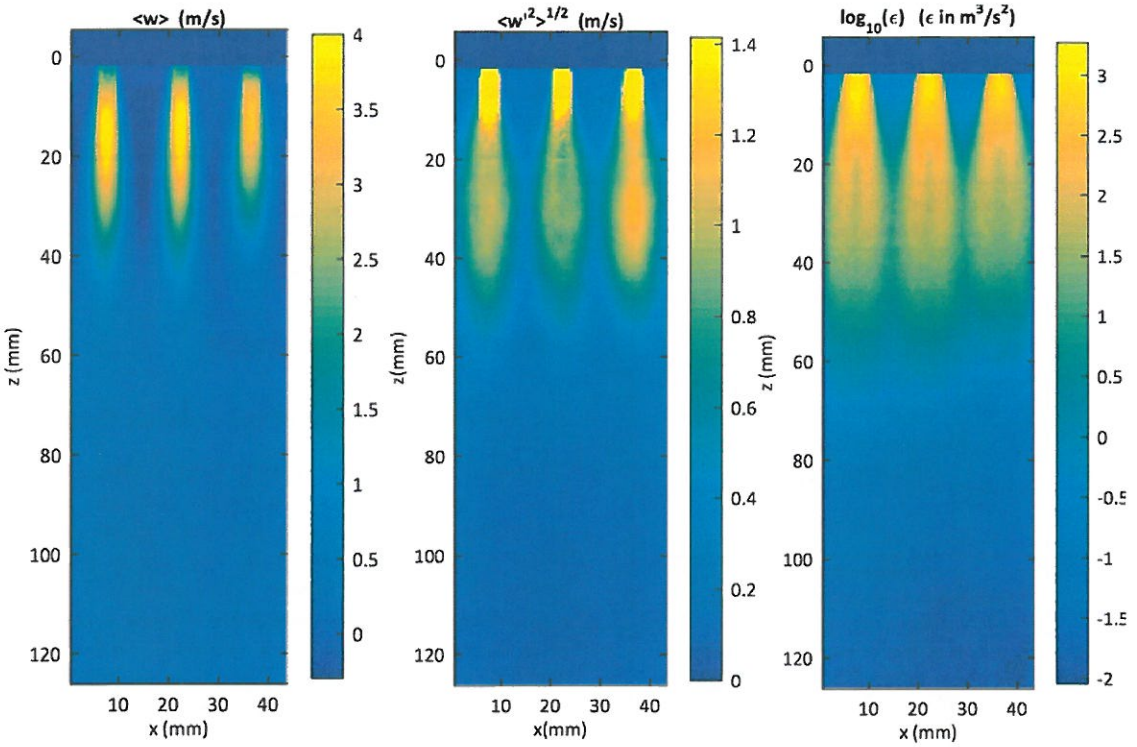

Fig. 3. Measured velocity field in the plane below nozzle centers. Left: mean vertical velocity. Middle: fluctuating component of vertical velocity. Right: local dissipation rate of turbulent energy.

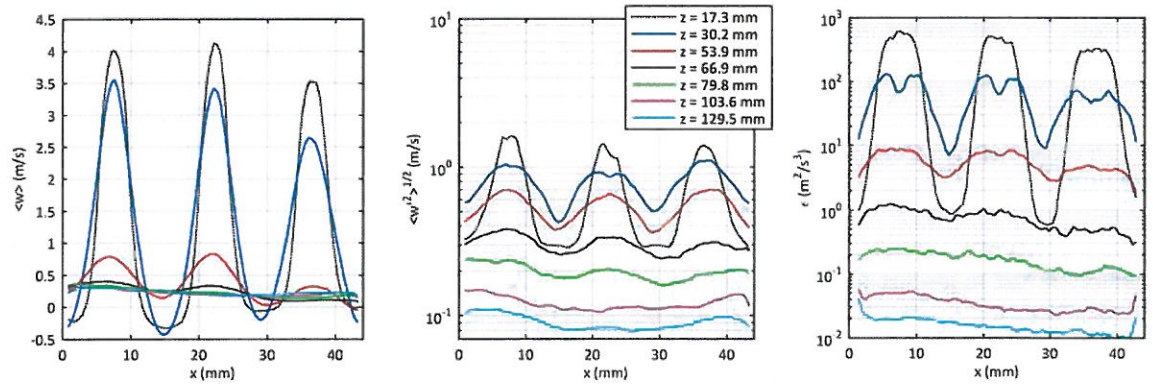

Fig. 4. Profiles of mean velocity, fluctuating component and local dissipation rate for several cross-section of fields shown in previous figure.

showing that most of the injected kinetic energy is dissipated within the cell. Results are presented in Table 2. Apparently, the present method "sees" about one half of the energy dissipation in all measured cases, and this disagreement could be fixed by adjusting either Smagorinsky constant C_S or the filter size Δ in (1) appropriately.

Table 2. Comparison of measured total dissipation and injected energy flux.

flow rate in inlet 1 (L/min)	dissipated energy (W)	inlet energy flux (W)	ratio (-)
20	0.145	0.306	0.474
48	2.06	4.11	0.502
68	6.38	11.7	0.546
88	10.8	25.3	0.427

3.2. Velocity difference statistic

The probability density function of longitudinal velocity difference δw in two points is shown in Fig. 7. Multiple p.d.f.'s are shown, each of them is for a different vertical position. As expected, broader distributions are observed close to the nozzles, where velocity fluctuations are high, and they are becoming narrower downstream. Different p.d.f.'s are observed when the separation distance d, for

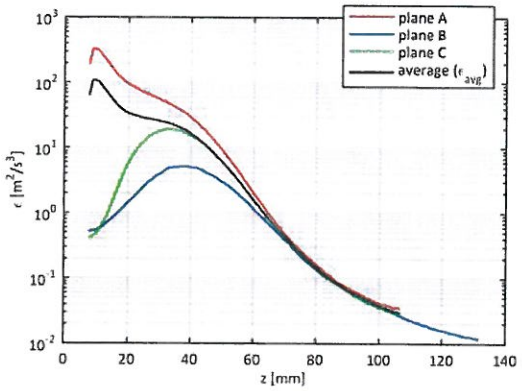

Fig. 5. Longitudinal profiles of local dissipation rate

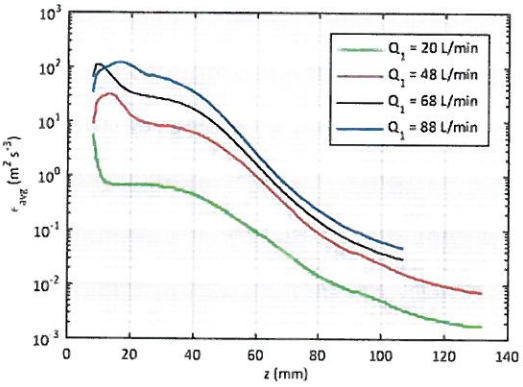

Fig. 6. Comparison of averaged profiles of dissipation rate for several flow conditions

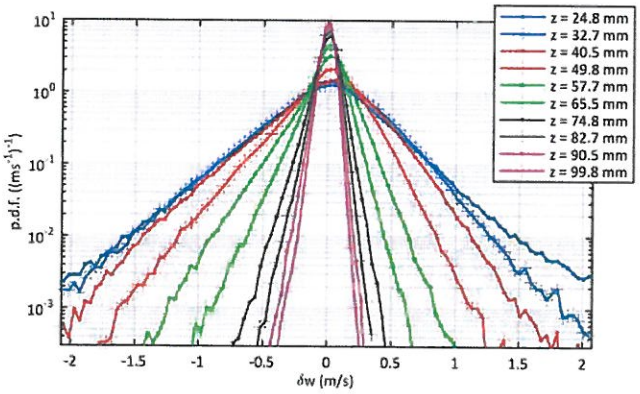

Fig. 7. Probability density function for the longitudinal velocity difference in two points separated by distance $d = 2.07$ mm.

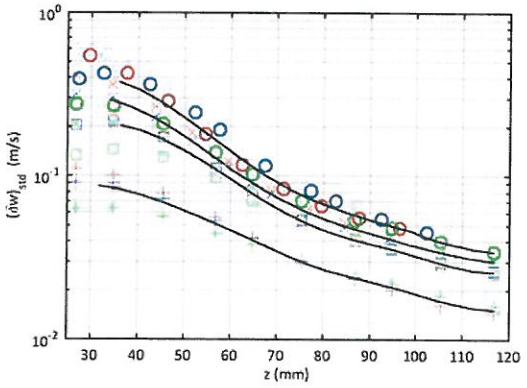

Fig. 8. Standard deviation of longitudinal velocity difference for separation $d = 2.07$ mm. Red, blue and green symbols are for planes A, B and C, respectively. Symbols +, □, x and ○ are for $Q_1 = 20$, 48, 68 and 88 L/min, respectively. Black lines are the average valued for all three planes.

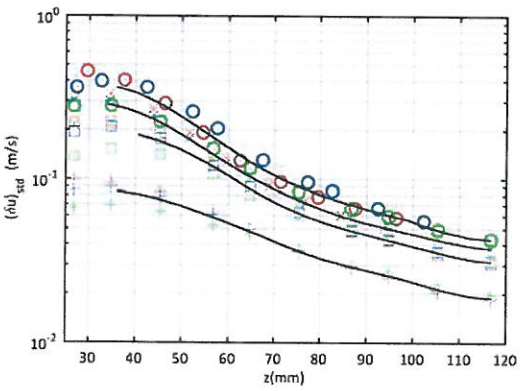

Fig. 9. Same as previous figure, but for transversal velocity difference.

which the velocity difference statistics is evaluated, is changed. The p.d.f. of velocity difference hence depends on position, on the separation distance d, and on the flow conditions.

The width of the p.d.f. is characterized by its second moment, that is by the standard deviation of the velocity difference, $(\delta u)_{std}$ and $(\delta w)_{std}$. Their evolutions are shown in Figs. 8 and 9 for longitudinal and transversal velocity difference.

All p.d.f.'s almost collapse to a single master distribution, when either δu or δw is normalized by its standard deviation. This is shown in Figures 10 and 11 for the longitudinal and transversal velocity difference, respectively.

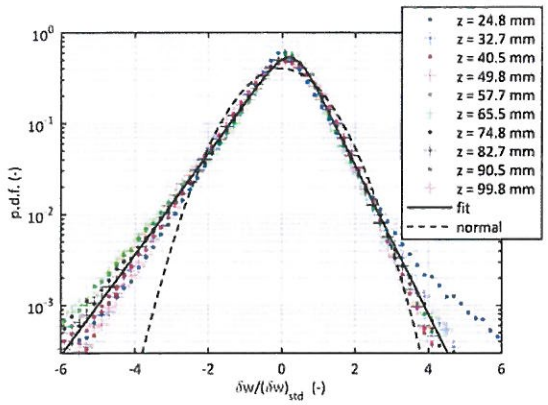

Fig. 10. Probability density function for normalized longitudinal velocity difference in two points separated by distance $d = 2.07$ mm.

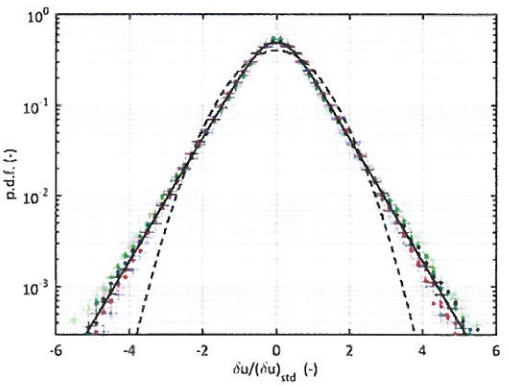

Fig. 11. Probability density function for normalized transversal velocity difference in two points separated by distance $d = 2.07$ mm.

These p.d.f.'s are non-Gaussian (compare them to normal distribution shown by dashed black line). In the case of longitudinal velocity component, the p.d.f. is skewed; this is expected because of the vertical gradient in the turbulent energy. Both master p.d.f.'s have high kurtosis, indicating that extreme velocity differences are observed quite frequently in the flow. The tails of velocity difference distributions are almost exponential (straight line in semi-logarithmic representation in Figs. 10 and 11). The character of the p.d.f. of δu is similar to that reported by Jung and Swinney [18].

When the distance d, for which the velocity statistics is evaluated, is changed, p.d.f.'s of the velocity difference still sticks to the same master distribution, but the standard deviation varies as $\delta w_{std} \sim d^{0.62}$ (and similarly $\delta u_{std} \sim d^{0.62}$), which is close to the theoretical dependence $\sim d^{2/3}$ found for homogeneous isotropic turbulence.

The collapse of all velocity difference p.d.f.'s to the single master curve has enormous practical implication for experiments on particle breakup: it is sufficient to characterize the standard deviation δw_{std} for a given separation distance d, and complete p.d.f. of δw for any distance d can then be reconstructed.

4 Conclusions

The velocity field in a turbulent cell, in which break-up of fluid particles is studied, has been characterized by means of PIV. The characterization has focused on the local dissipation rate (which is a commonly used parameter in modelling of the breakup), and on the statistics of the velocity difference in two points.

The local dissipation rate has been estimated by means of Large-Eddy PIV. The estimation has been validated by comparing the total dissipation rate to the energy influx to the experimental cell. The validation indicates that LEPIV "sees" about one half of the total dissipation rate.

The two-point velocity differences have non-Gaussian probability-density function. These p.d.f. are same everywhere, if normalized by standard deviation of the velocity difference. This standard deviation is proportional to the two-third power of distance between the points, for which it is evaluated.

Acknowledgement: This research has been supported by Czech Science Foundation (project no. 15-15467S).

References

1. J. Solsvik and H. A. Jakobsen, Rev. Chem. Eng. **29**, 63 (2013).
2. J. Solsvik, S. Tangen, and H. A. Jakobsen, Rev. Chem. Eng. **29**, 241 (2013).
3. J. C. Lasheras, C. Eastwood, C. Martinez-Bazan, and J. L. Montanes, Int. J. Multiphase Flow **28**, 247 (2002).
4. J. Solsvik and H. A. Jakobsen, Int. J. Chem. Reactor Eng. **13**, 477 (2015).
5. S. Maass and M. Kraume, Chem. Eng. Sci. **70**, 146 (2012).
6. S. Maass, N. Paul, and M. Kraume, Chem. Eng. Sci. **76**, 140 (2012).
7. F. Ravelet, C. Colin, and F. Risso, Phys. Fluids **23**, 103301 (2011).
8. F. Risso and J. Fabre, J. Fluid Mech. **372**, 323 (1998).
9. R. Andersson and B. Andersson, Aiche J. **52**, 2020 (2006).
10. C. Martinez-Bazan, J. L. Montanes, and J. C. Lasheras, J. Fluid Mech. **401**, 157 (1999).
11. C. Martinez-Bazan, J. L. Montanes, and J. C. Lasheras, J. Fluid Mech. **401**, 183 (1999).
12. M. Zednikova, J. Vejrazka, and P. Stanovsky, in Experimental Fluid Mechanics (Mariánské Lázně, 2016).
13. J. Vejrazka, PIVsuite (2014), http://www.mathworks.com/matlabcentral/fileexchange/45028-pivsuite
14. M. Stanislas, K. Okamoto, C. J. Kahler, J. Westerweel, and F. Scarano, Exp. Fluids **45**), 27 (2008).
15. J. Sheng, H. Meng, and R. O. Fox, Chem. Eng. Sci. **55**, 4423 (2000).
16. J. Smagorinsky, Monthly Wheather Review **91**, 99 (1963).

17. J. de Jong, L. Cao, S. H. Woodward, J. Salazar, L. R. Collins, and H. Meng, Exp. Fluids **46**, 499 (2009).
18. S. W. Jung and H. L. Swinney, Phys. Rev. E **72**, 026304 (2005).